Specific regulation of thermosensitive lipid droplet fusion by a nuclear hormone receptor pathway

Shiwei Li[a], Qi Li[a], Yuanyuan Kong[a], Shuang Wu[a], Qingpo Cui[a], Mingming Zhang[a], and Shaobing O. Zhang[a,1]

[a]Laboratory of Metabolic Genetics, College of Life Sciences, Capital Normal University, Beijing 100048, China

Edited by David W. Russell, University of Texas Southwestern Medical Center, Dallas, TX, and approved July 10, 2017 (received for review March 14, 2017)

Nuclear receptors play important roles in regulating fat metabolism and energy production in humans. The regulatory functions and endogenous ligands of many nuclear receptors are still unidentified, however. Here, we report that CYP-37A1 (ortholog of human cytochrome P450 CYP4V2), EMB-8 (ortholog of human P450 oxidoreductase POR), and DAF-12 (homolog of human nuclear receptors VDR/LXR) constitute a hormone synthesis and nuclear receptor pathway in *Caenorhabditis elegans*. This pathway specifically regulates the thermosensitive fusion of fat-storing lipid droplets. CYP-37A1, together with EMB-8, synthesizes a lipophilic hormone not identical to Δ7-dafachronic acid, which represses the fusion-promoting function of DAF-12. CYP-37A1 also negatively regulates thermotolerance and lifespan at high temperature in a DAF-12–dependent manner. Human CYP4V2 can substitute for CYP-37A1 in *C. elegans*. This finding suggests the existence of a conserved CYP4V2-POR–nuclear receptor pathway that functions in converting multilocular lipid droplets to unilocular ones in human cells; misregulation of this pathway may lead to pathogenic fat storage.

nuclear receptor | thermosensitive lipid droplet fusion | CYP-37A1 | EMB-8 | DAF-12

A major challenge in the understanding of nuclear receptor signaling is to identify the specific ligands and physiological functions of orphan receptors at the molecular and subcellular level. In human, essentially all known endogenous steroid and nonsteroid hormones for nuclear receptors are synthesized by members of a large family of 50 microsomal cytochrome P450 monooxgenases, which require a common P450 oxidoreductase (POR) to carry out their catalysis. Many of these putative hormone-synthesizing enzymes are also of unknown function (1). Typically, the binding of hormone ligands to cognate nuclear receptors leads to both down-regulation of the expression of P450s and inactivation of the ligands, maintaining signaling homeostasis. For this reason, P450s are acclaimed as the "unsung heroes" of the P450–hormone–nuclear receptor signaling axis (2). Research on orphan P450s will likely lead to important discoveries of human nuclear receptor signaling and physiology.

The genome of the nematode *Caenorhabditis elegans* encodes 284 nuclear receptors, 82 P450s, and a single POR (EMB-8) (3–5), suggestive of a large repertoire of nuclear hormone receptor signaling. Among the 284 nuclear receptors, only one, DAF-12, has so far been linked to endogenous hormone ligands, the bile acid-like steroids Δ7 and Δ1,7-dafachronic acids (DAs) (6–8). DAs are synthesized by a P450 DAF-9 (i.e., CYP-22A1) with help from EMB-8/POR in addition to a Rieske-like oxygenase DAF-36 and a 3-hydroxysteroid dehydrogenase DHS-16 (9–11). When DAs are absent, DAF-12 recruits a transcriptional coregulator, DIN-1, to regulate genes that promote the formation of dauer, an alternative life form resistant to harsh environments. In contrast, DA-bound DAF-12 regulates the transcription of a different set of genes to promote reproductive growth and accelerate aging (12, 13). Thus, DAF-9–DAs–DAF-12–DIN-1 represents the only delineated P450–hormone–nuclear receptor pathway with clear physiological functions in *C. elegans*. This pathway is similar to the synthesis of bile acids that serve as ligands for farnesoid X receptor (FXR) in mammals (14).

Upon binding to DAs, DAF-12 also activates genes involved in fatty acid oxidation for energy production (15). However, it is not understood how DAF-12 signaling and metabolic flux converge on the subcellular fat-storing structures to regulate fat deposition and mobilization. In eukaryotes, fat is stored in a class of newly defined cell organelles called lipid droplets (LDs), whose morphological and metabolic status plays active roles in fat metabolism (16). Previously, we identified that the subcellular fat-storing structures of *C. elegans* are LDs (17, 18). By applying reliable and effective LD labeling methods to a systematic and saturated forward genetic screen, we isolated four classes of *drop* (lipid droplet abnormal) mutants that form supersized LDs in intestine cells (19). Here, we cloned two class III mutants, *drop-1* and *drop-8*, and their suppressor mutant *drop-31*. We show that the three genes constitute a P450–nuclear receptor pathway.

Results

CYP-37A1 and EMB-8 Negatively Regulate Thermosensitive Supersized LD Formation. When fed ad libitum, wild-type (WT) *C. elegans* produces triacylglycerol (TAG)-storing LDs with an upper size limit of 3 μm in diameter (17, 18). We previously isolated two class III supersized LD mutants, *drop-1* and *drop-8* (19), which upon a shift from 15/20 °C to 30 °C, quickly form supersized LDs ≥ 3 μm. We have now cloned *drop-1* and *drop-8* as *cyp-37A1* and *emb-8*, respectively (Fig. S1 *A* and *B*). CYP-37A1 is orthologous to human CYP4V2; as mentioned above, EMB-8 is orthologous to POR.

The 38 alleles of *cyp-37A1* that we isolated include deletion, splicing, nonsense, and missense mutations (Fig. S1 *A* and *C*). Together with a 1,234-bp deletion allele, *ok673*, all alleles display a fully penetrant and strict temperature-sensitive supersized LD phenotype as revealed by postfix Oil Red O staining (Fig. 1 *A*–*D*), indicating null mutations. Only one *emb-8* allele, *ssd89* (G22D), was previously isolated (19). *ssd89*(G22D) displays a fully penetrant supersized LD phenotype (Fig. 1 *E* and *F*). We have now used a noncomplementation screen strategy to isolate

Significance

Human and animals store fat in the form of multiple small intracellular structures, called lipid droplets, in brown adipocytes, and in a single large lipid droplet in white adipocytes. When environmental temperature decreases, white adipocytes can convert into brown adipocytes, in which fat is more accessible for burning and thermogenesis, and vice versa. The mechanism underlying the interconversion between multiple and single lipid droplets is not clear. Here, we report that a nuclear hormone signaling pathway regulates similar conversions in the nematode *Caenorhabditis elegans*, and that components of this pathway have counterparts in humans.

Author contributions: S.L. and S.O.Z. designed research; S.L., Q.L., Y.K., S.W., Q.C., M.Z., and S.O.Z. performed research; S.L. and S.O.Z. analyzed data; and S.O.Z. wrote the paper.

The authors declare no conflict of interest.

This article is a PNAS Direct Submission.

[1]To whom correspondence should be addressed. Email: soz001@cnu.edu.cn.

This article contains supporting information online at www.pnas.org/lookup/suppl/doi:10.1073/pnas.1704277114/-/DCSupplemental.

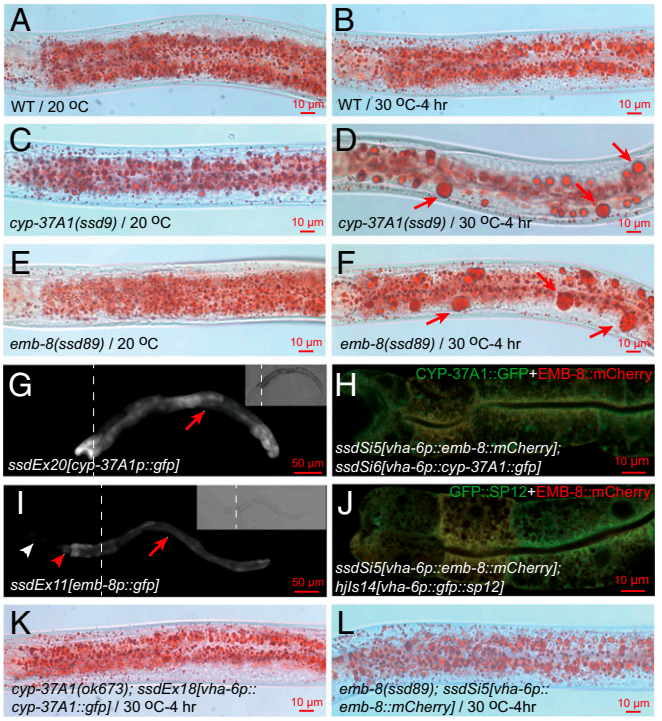

Fig. 1. Mutations of CYP-37A1 and EMB-8 cause supersized LD formation. (*A* and *B*) WT animals grown continuously at 20 °C to mid-L4 stage, or shifted from 20 °C to 30 °C for 4 h before reaching the mid-L4 stage, have no supersized LDs (≥3 μm in diameter). Images are of postfix Oil Red O staining. (*C* and *D*) When shifted to 30 °C for 4 h, *cyp-37A1(ssd9)* forms supersized LDs (arrows) and reduces the number of LDs smaller than 3 μm; (*E* and *F*) as in *C* and *D*, so does *emb-8(ssd89)*. (*G*) *cyp-37A1* (*ssdEx20*) is specifically expressed in intestine cells (arrow). (*Inset*) Bright field. (*H*) CYP-37A1::GFP protein (*ssdSi6*) colocalizes with EMB-8::mCherry (*ssdSi5*). (*I*) *emb-8* (*ssdEx11*) is expressed in intestine (arrow), pharynx (red arrowhead), and neurons surrounding the first pharyngeal bulb (white arrowhead). (*J*) EMB-8::mCherry (*ssdSi5*) colocalizes with an ER marker GFP::SP12 (*hjIs14*). (*K*) Intestinal expression of CYP-37A1::GFP (*ssdEx18*) completely rescues *cyp-37A1(ok673)*. (*L*) Intestinal expression of EMB-8::mCherry (*ssdSi5*) completely rescues *emb-8(ssd89)*. For (*G*) and (*I*), GFP and bright field images are montages of two images (dashed lines indicate boundaries) covering the anterior and posterior parts of the same animal sample. For each Oil Red O experiment, more than 50 mid-L4–stage animals were stained and examined and at least 20 were imaged. Images are of the anterior half of the animal with head to the left. The same applies to other Oil Red O experiments, if not otherwise indicated.

three additional alleles with a similar supersized LD phenotype (Fig. S1*B*). We constructed two transgenic lines, *ssdEx20* and *ssdEx21*, in which a 1,259-bp *cyp-37A1* promoter drives GFP reporter expression. The result shows that *cyp-37A1* is specifically expressed in intestine cells (Fig. 1*G*). In another experiment, we constructed two transgenic lines, *ssdEx17* and *ssdEx18*, in which a CYP-37A1::GFP fusion protein is driven by an intestine-specific promoter *vha-6p*. Both *ssdEx17* and *ssdEx18* rescued the supersized LD phenotype of *cyp-37A1(ok673)* (Fig. 1*K*). To investigate the subcellular localization of CYP-37A1 protein, we created a single-copy transgenic line *ssdSi6* to express CYP-37A1::GFP driven by *vha-6p* using the MosSCI technology (20). The result shows that CYP-37A1::GFP localizes in a pattern characteristic of the endoplasmic reticulum (ER) (Fig. 1*H*). With similar experiments, we found that: *emb-8* is expressed in the intestine, pharynx, and neurons surrounding the first pharyngeal bulb (Fig. 1*I*); transgenic EMB-8::mCherry protein colocalizes with CYP-37A1::GFP and an ER marker GFP::SP12; and EMB-8::mCherry rescues *emb-8(ssd89)* when expressed in the intestine (Fig. 1 *H*, *J*, and *L*).

CYP-37A1 and EMB-8 Mutations Derepress a Nonasymmetric and Thermosensitive LD Fusion Process. To test the mechanism of supersized LD formation, we time-lapse–imaged GFP::DGAT-2-labeled LDs in live *cyp-37A1(ssd2)* animals shifted to 30 °C. In 21 time-lapse movies, 57 LD fusion events but no single LD growth event was found. Similar to what was reported before (19), all fusion events happened in a time window shorter than 30 s and displayed no asymmetric partnership (Movie S1 and S2). The sizes of the two fusing LDs displayed no asymmetry either along the mediolateral or along the anteroposterior polarity axis of intestine cells (Fig. 2 *A–D*). To test whether the supersized LD phenotype of the mutants can be attributed to increased LD growth, we used lipid extraction and quantitative lipid analytical chemistry to measure the TAG levels. As shown by the results, at 20 °C, *cyp-37A1(ssd9)*, *emb-8(ssd89)*, and WT animals stored similar amounts of TAG. After being shifted to 30 °C for 4 h, *emb-8(ssd89)* had no increase in TAG, while *cyp-37A1(ssd9)* and WT had a modest decrease (Fig. 2*E*). Furthermore, fasting experiments showed that small and supersized LDs formed before and after temperature shift in the mutants are liable to hydrolysis, with no obvious difference to LDs in WT (Fig. S2), ruling out the possibility that the supersized LDs are a result of decreased LD hydrolysis.

We used genetic analyses to test whether the supersized LD phenotype is dependent on TAG synthesis, lipogenesis, or other

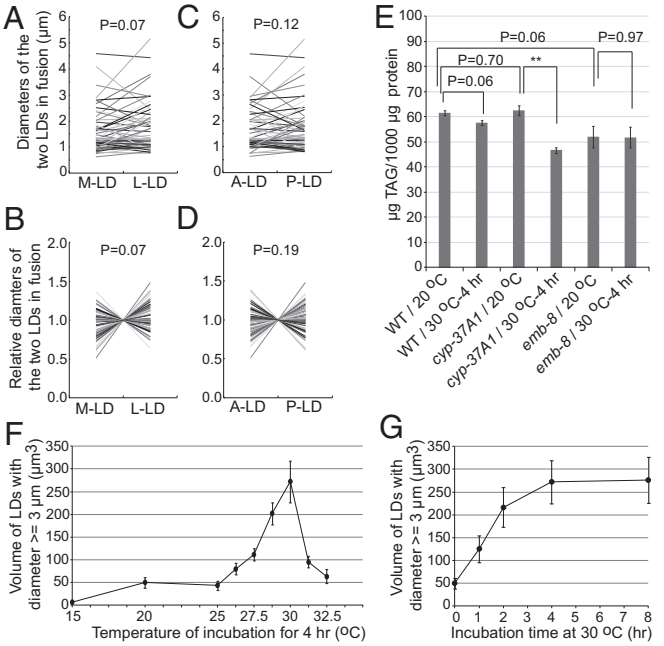

Fig. 2. Mutation of *cyp-37A1* derepresses a nonasymmetric and thermosensitive LD fusion process. (*A–D*) The two fusing LDs are designated as medial (M) vs. lateral (L), or anterior (A) vs. posterior (P). The absolute diameters of the two LDs (*A* and *C*) and relative diameters normalized to the mean (*B* and *D*) are plotted as connecting lines. No significant size asymmetry is found between the two LDs. Paired two-sample *t* test. $n = 57$. (*E*) There is no significant difference of TAG level between WT and *cyp-37A1 (ssd9)/emb-8(ssd89)*, between before and after fusion for WT and *emb-8 (ssd89)*. There is a small but significant decrease after fusion for *cyp-37A1 (ssd9)*. Data are mean ± SEM. $n = 3$ for WT and *cyp-37A1(ssd9)*; $n = 7$ for *emb-8(ssd89)*. $^{**}P \leq 0.01$. Unpaired two-sample *t* test. (*F* and *G*) The volume of supersized LDs formed in the second intestine in *cyp-37A1(ssd2); glo-4 (ok623)* is used to quantitate the fusion rate upon different temperature treatment or with different treatment time. Fusion starts at 25 °C, peaks at 30 °C, and declines beyond 30 °C (*F*). Fusion in *cyp-37A1(ssd2); glo-4(ok623)* increases over time and plateaus at 4 h, displaying a first-order kinetics (*G*). Data are mean ± SEM. $n \geq 10$.

factors. As shown by postfix Oil Red O experiments on double mutants, the formation of supersized LDs of *cyp-37A1(ssd9)* and *emb-8(ssd89)* is not dependent on the LD growth-mediating ACS-22-DGAT-2 enzyme complex (17, 21), the lipogenic transcription factor SBP-1 (22), or the ER GTPase ATLN-1 (23) (Fig. S3 *A–H*). We also measured the phospholipid compositions of WT and mutants. The results showed that, compared with WT, *cyp-37A1(ssd9)* and *emb-8(ssd89)* do not show any obvious alteration in the relative amount of phosphatidylcholine or other phospholipids (Fig. S4).

The null nature of *cyp-37A1* alleles indicates that LD fusion is not a result of thermosensitive loss of CYP-37A1 enzyme function, but rather an up-regulation of a thermosensitive process. We used the LD marker GFP::DGAT-2, vital BODIPY staining, and vital BODIPY staining combined with a lysosome-related organelle-negative *glo-4(ok623)* mutant background to label LDs in WT and mutants (18, 19). We confocal-imaged these animals in three dimensions and quantified the volume of supersized LDs as an index of fusion process. The different labeling methods yielded the same result. In WT, no supersized LDs (diameters ≥ 3 μm) formed. In both *cyp-37A1(ssd2)* and *cyp-37A1(ssd9)* mutants, supersized LDs formed; the total volume of all supersized LDs formed in the two cells of the second intestine segment reaches ∼300 μm^3 (Fig. S5). This volume can be approximated as 10 fusion events of LDs 3 μm in diameter in each cell, certainly an underestimation since small LDs (diameters < 3 μm) also fuse (Fig. 2*A*). We then used confocal imaging to quantify temperature dependence and reaction time course of the fusion process. As shown by the LD volume data, the fusion is temperature-dependent; it is first evident at 25 °C, peaks at 30 °C, and decreases beyond 30 °C (Fig. 2*F*). The fusion process also exhibits first order kinetics: the number of fusion events increases over time and plateaus at 4 h (Fig. 2*G*), when most small LDs are consumed (Fig. 1 *D* and *F* and Fig. S5 *D–F*).

All of these results demonstrate that *cyp-37A1* and *emb-8* mutants form supersized LDs not through LD growth or lipogenesis but through a direct, thermosensitive, fast, and nonasymmetrical fusion process. The function of WT CYP-37A1 and EMB-8 is to repress this thermosensitive LD fusion process.

CYP-37A1 Is a Functional Ortholog of Human CYP4V2 and Represses Thermosensitive LD Fusion Without Affecting the Bulk Fatty Acid Composition. The LD fusion repression function must lie in the specificity of CYP-37A1, which should function at the same biochemical and genetic level as EMB-8, the general electron donor for all microsomal P450s. Consistent with this notion, the double-mutant *cyp-37A1(ssd9); emb-8(ssd89)* has a similar phenotype to each single mutant (Fig. S3*I*). At the protein sequence level, *C. elegans* CYP-37A1 is orthologus to human CYP4V2 and most of the missense mutations of CYP-37A1 are after amino acid residues that are conserved in CYP4V2 (Fig. S1*C*). We synthesized a synonymous CYP4V2 cDNA optimized for *C. elegans* codon use (24), and made two transgenic lines, *ssdEx51* and *ssdEx52*, that express CYP4V2::GFP protein in intestine (Fig. S6*A*). In both lines, human CYP4V2 rescues the LD fusion phenotype of *cyp-37A1(ssd9)* (Fig. S6 *B* and *C*). Thus, CYP-37A1 and CYP4V2 are functional orthologs.

CYP4V2 mutation is a risk factor for human Biette crystalline corneoretinal dystrophy (BCD), a chronic, severe eye disease that is marked by the pathological formation of glistening lipid inclusions with an unknown etiology in retinal pigment epithelium cells (RPEs) (25, 26). CYP4V2 ω-hydroxylates fatty acids in vitro and in a heterologous cell system and is thought to degrade bulk fatty acids in RPEs (27–30). Thus, to test the possibility that CYP-37A1 mutants affect the fatty acid composition in *C. elegans*, we used lipid analytical chemistry to quantitate fatty acid compositions of WT and the LD fusion mutants *cyp-37A1 (ssd9)* and *emb-8(ssd89)*. WT and *cyp-37A1(ssd9)* grown in parallel under the same food condition were not obviously different in TAG fatty acid composition, before or after LD fusion (Table S1). Changing the growth time of the OP50 *Escherichia coli* food on nematode growth medium (NGM) affects the fatty acid compositions of OP50, and then of *C. elegans*. This change does not affect the LD fusion phenotype of *cyp-37A1(ssd9)* and *emb-8(ssd89)*. On such a different batch of food, WT and *emb-8 (ssd89)* grown in parallel were both different to WT grown on the other batch of food in TAG fatty acid composition; but WT and *emb-8(ssd89)* were not different from each other (Table S1). Finally, when grown under the same food condition in parallel, WT, *cyp-37A1(ssd9)*, and *emb-8(ssd89)* showed no consistent difference in total fatty acid composition (Table S1). Thus, we conclude that the role of CYP-37A1 and EMB-8 is not for the degradation of bulk fatty acids.

CYP-37A1 and EMB-8 Synthesize a Lipophilic Hormone to Repress DAF-12–Mediated LD Fusion. It is possible that CYP-37A1, together with EMB-8, modifies fatty acids or other lipid molecules to generate trace amount of bioactive metabolites that exert a signaling role. To investigate this possibility, we conducted *cyp-37A1(ssd9)* suppressor screens. We identified a suppressor group *drop-31* with two alleles. Molecular cloning showed that *drop-31* is mutated in the nuclear receptor gene *daf-12* (*Materials and Methods*). *daf-12(ssd155)* and *daf-12(ssd240)* are nonsense mutations that abolish both the ligand binding domain and the transactivation domain (6), and thus are likely to be null mutants. *daf-12(ssd155)*, *daf-12(ssd240)*, and a known nonsense null mutation *daf-12(m583)*, completely suppress LD fusion in *cyp-37A1(ssd9)* and *emb-8(ssd89)* (Fig. 3 *A–D* and Table 1). This result suggests that DAF-12 mediates the LD fusion activity that is derepressed in *cyp-37A1(ssd9)* and *emb-8(ssd89)*, and that WT CYP-37A1 synthesizes a lipophilic hormones to repress DAF-12. To test this idea, we prepared a total lipid extract equivalent to 6 mg total protein (defined as 1X) from WT animals and found that applying the 1X lipid extract to intact *cyp-37A1(ssd9)* animals suppressed the LD fusion phenotype by 50.8%. In contrast, the 1X lipid extract from *cyp-37A1(ssd9)* suppressed *cyp-37A1 (ssd9)* by only 5.3%. Delipidated extracts showed no activity in this assay (Fig. 3 *E* and *F* and Table 1).

DAF-12 mediates the decision between reproductive development and dauer diapause; reproductive development is promoted by the presence of hormone ligands, known as DAs, whereas dauer formation is promoted by the absence of DAs (7, 8). Is DA the putative hormone synthesized by CYP-37A1? To address this question, we supplemented populations of *cyp-37A1 (ssd9)* mutants with the classic DAF-12 ligand Δ7-DA (at concentrations of 0.02, 0.2, 2 μM) to test its effect on LD fusion. The results showed that Δ7-DA does not suppress LD fusion in *cyp-37A1(ssd9)* at the L3 stage but partially suppresses it at the L4 stage. However, the partial suppression at L4 is associated with a depletion of LDs rather than a block of LD fusion (Fig. 3 *G* and *H*). Moreover, the effect is nonlinear with Δ7-DA concentration (Table 1 and Fig. S7).

One explanation for these observations is that DAF-12 is acted upon by two functionally distinct ligand types: (*i*) the previously described DAs that inhibit dauer formation and promote lipolysis (15); and (*ii*) a novel hormone ligand that inhibits thermosensitive LD fusion. Consistent with this reasoning, the DA-defective mutants, *daf-9(e1406)*, *daf-36(k114)*, and the DA binding-defective mutant, *daf-12(rh274)*, already form supersized LDs at 20 °C. However, in these three mutants, the formation of supersized LDs at 20 °C is not coincident with a decrease of small LDs (i.e., it is characteristic of LD growth instead of LD fusion). Moreover, supersized LDs or small LDs do not fuse when the three mutants are shifted to 30 °C (Fig. S8 *A–F*). Finally, the LD growth/lipogensis phenotype of *daf-9(e1406)* and *daf-36(k114)* is largely suppressed by the supplementation of

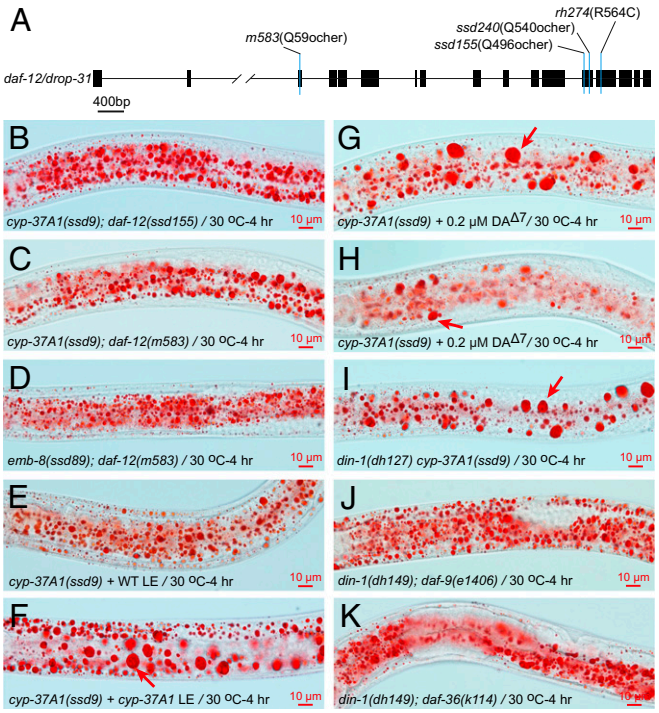

Fig. 3. DAF-12 mediates LD fusion in *cyp-37A1* and *emb-8* mutants. (*A*) The two *drop-31* alleles, *ssd155* and *ssd240*, are nonsense mutants of *daf-12*. *m583* and *rh274*, two other *daf-12* mutants, are null and gain-of-function (dauer-constitutive), respectively. (*B–D*) Null mutations of *daf-12* completely suppress LD fusion of *cyp-37A1(ssd9)* and *emb-8(ssd89)*. (*E* and *F*) A total lipid extract (LE) of WT but not of *cyp-37A1(ssd9)* suppresses LD fusion in *cyp-37A1(ssd9)* animals. (*G*) A supplementation of 0.2 μM Δ7-DA does not suppress LD fusion but occasionally decreases the amount of LDs in *cyp-37A1 (ssd9)* (*H*). (*I*) *din-1(dh127)* does not suppress *cyp-37A1(ssd9)*. (*J* and *K*) *din-1 (dh149)* completely suppresses the supersized LD phenotype of *daf-9(e1406)* and *daf-36(k114)*.

0.2 μM Δ7-DA and is completely suppressed by 2 μM Δ7-DA (Table 1 and Fig. S8 *G–J*). Thus, the role of DA in LD regulation differs from that of the postulated hormone synthesized by CYP-37A1.

In the DA-defective mutants *daf-9(e1406)* and *daf-36(k114)*, the prodauer function of DAF-12 requires the transcription cofactor DIN-1 (12). If DA synthesized by DAF-9/DAF-36 and the hormone synthesized by CYP-37A1 differentially regulate LD growth/lipogenesis and LD fusion, *daf-9*/*daf-36* and *cyp-37A1* mutants may differ in their DIN-1 dependence. Our results showed that this indeed is the case: when DIN-1 is dysfunctional, *daf-9(e1406)*, *daf-36(k114)*, and *daf-12(rh274)* do not form supersized LDs at 20 °C or when shifted to 30 °C (Fig. 3 *J* and *K*, Table 1, and Fig. S9 *A–D*); in contrast, when DIN-1 is dysfunctional, *cyp-37A1(ssd9)* still forms supersized LDs via thermosensitive fusion with a nearly full penetrance (Fig. 3*I* and Table 1).

To further test the differential roles of the hormone synthesized by CYP-37A1 and of DA, we compared double-mutant *din-1(dh127) cyp-37A1(ssd9)* (DA-present) and triple mutants *din-1 (dh127) cyp-37A1(ssd9); daf-9(e1406)* and *din-1(dh149) cyp-37A1 (ssd9); daf-36(k114)* (DA-deficient). The results showed that, with or without DAF-36, LD fusion in *din-1(dh127) cyp-37A1 (ssd9)* is normal. With the presence of DAF-9, LD fusion in *din-1 (dh127) cyp-37A1(ssd9)* is normal; without DAF-9, LD fusion in *din-1(dh127) cyp-37A1(ssd9)* is not enhanced but is partially impaired, indicating an unexpected cross-talk between CYP-37A1 and DAF-9 at the level of DAF-12 (Fig. 3*I*, Table 1, and Fig. S9 *E–H*).

***cyp-37A1* Mutant Tolerates Heat Stress in a DAF-12–Dependent Manner.** The thermosensitive LD fusion regulated by CYP-37A1 and DAF-12 may be linked to heat adaptation for *C. elegans* in its natural habitat. To test this hypothesis, we measured the survival rates of WT and *cyp-37A1(ssd9)* 1-d-adult animals upon exposure to 34 °C. The results showed that both WT and *cyp-37A1(ssd9)* start to die by 2-h exposure and that no animal survived an 8-h exposure (Fig. 4*A*). However, at the 4-h time point, the survival rate of *cyp-37A1(ssd9)* was much higher than WT. The increased survival of *cyp-37A1(ssd9)* is partially dependent on DAF-12 (Fig. 4*B*). We also measured the lifespans of WT and *cyp-37A1(ssd9)*. At 20 °C, the mean lifespan of *cyp-37A1 (ssd9)* is slightly longer (~2 d longer) than that of WT. The extended lifespan of *cyp-37A1(ssd9)* is dependent on DAF-12 (Fig. 4*C*). At 25 °C, lifespans of both WT and *cyp-37A1(ssd9)* are shortened. However, the mean lifespan of *cyp-37A1(ssd9)* is much longer (~5 d longer) than that of WT. The extended lifespan is completely dependent on DAF-12 (Fig. 4*D*). These results demonstrate that *cyp-37A1* mutants have a better tolerance of acute heat stress and ambient heat stress in a DAF-12–dependent manner.

Table 1. Epistasis analysis of the supersized LD phenotype

Genotype and treatment	% SLD^{+}	*n*
cyp-37A1(ssd9)	100	109
cyp-37A1(ssd2)	100	100
cyp-37A1(ok673)	100	97
emb-8(ssd89)	98.8	83
cyp-37A1(ssd9); daf-12(ssd155)	0	62
cyp-37A1(ssd9); daf-12(m583)	1.0	97
emb-8(ssd89); daf-12(m583)	0	102
cyp-37A1(ssd9) + WT LE(1X)	49.2	61
cyp-37A1(ssd9) + WT LE(1X)-Del	100	73
cyp-37A1(ssd9) + *cyp-37A1(ssd9)* LE(1X)	94.7	95
cyp-37A1(ssd9) + *cyp-37A1(ssd9)* LE(1X)-Del	100	69
cyp-37A1(ssd9)+ DA$^{\Delta7}$(0.02 μM)	79.3	58
cyp-37A1(ssd9)+ DA$^{\Delta7}$(0.2 μM)	87.7	57
cyp-37A1(ssd9)+ DA$^{\Delta7}$(2 μM)	55.9	102
cyp-37A1(ssd9)+ DA$^{\Delta7}$(0.02 μM)*	98.4	63
cyp-37A1(ssd9)+ DA$^{\Delta7}$(0.2 μM)*	95.5	66
cyp-37A1(ssd9)+ DA$^{\Delta7}$(2 μM)*	90.2	61
daf-9(e1406)†	87	54
daf-9(e1406)+ DA$^{\Delta7}$(0.2 μM)†	3.4	58
daf-9(e1406)+ DA$^{\Delta7}$(2 μM)†	0	58
daf-36(k114)†	21.4	56
daf-36(k114) + DA$^{\Delta7}$(0.2 μM)†	14	57
daf-36(k114) + DA$^{\Delta7}$(2 μM)†	0	56
daf-12(rh274)	100	54
din-1(dh149); daf-12(rh274)	0	81
din-1(dh149); daf-9(e1406)	0	81
din-1(dh149); daf-36(k114)	0	87
din-1(dh127) cyp-37A1(ssd9)	94.2	104
din-1(dh127) cyp-37A1(ssd9); daf-9(e1406)	11.1	45
din-1(dh149) cyp-37A1(ssd9); daf-36(k114)	98.5	66

All data are of L4 stage animals shifted to 30 °C for 4 h unless otherwise indicated. % SLD^{+}, percentage of animals with supersized LDs. LE(1X), total lipid extract equivalent to 6 mg total protein. LE-Del, total lipid extract delipidated.
*Scored at L3 stage.
†Scored at 20 °C.

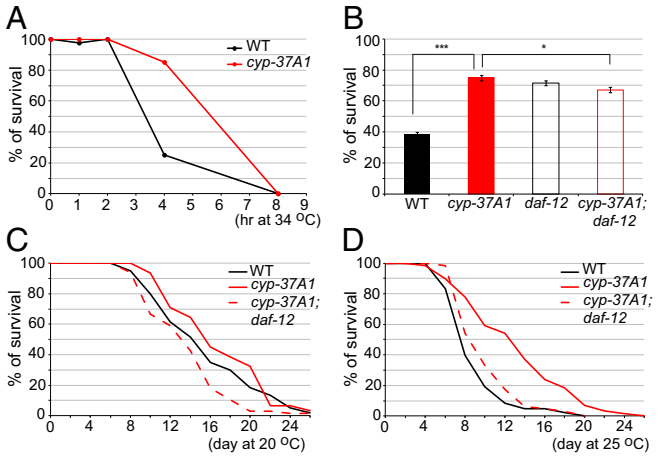

Fig. 4. Thermotolerance and lifespan. (*A*) WT and *cyp-37A1(ssd9)* 1-d adult animals started to die upon 2-h treatment of 34 °C. All animals died upon 8-h treatment. (*B*) Under a 34 °C/4-h treatment, the survival rate of *cyp-37A1 (ssd9)* is higher than that of WT. The better survival of *cyp-37A1(ssd9)* is partially impaired by *daf-12(m583)* mutation. Data are mean ± SEM of six replicates. ***$P < 0.001$, *$P \leq 0.05$, unpaired two-sample *t* test. (*C*) At 20 °C, the lifespan of *cyp-37A1(ssd9)* is slightly increased compared with that of WT. The lifespan increase of *cyp-37A1(ssd9)* is abolished by *daf-12(ssd155)* mutation. (*D*) At 25 °C, the lifespan of *cyp-37A1(ssd9)* is much increased than that of WT. The lifespan increase of *cyp-37A1(ssd9)* is abolished by *daf-12(ssd155)* mutation. Lifespan results are typical of two independent experiments.

Discussion

In summary, we have identified a hormone synthesis and nuclear receptor pathway consisting of CYP-37A1, EMB-8, and DAF-12 that regulates environment temperature-dependent LD fusion in the nematode *C. elegans*. This pathway shares components with the DAF-9–DAs–DAF-12 pathway (6, 7, 12), but differs from that pathway in three respects: (*i*) the DAF-12 hormone ligand synthesized by CYP-37A1 is not DA; (*ii*) DAF-12 does not require DIN-1 to exert its LD fusion-promoting function; and (*iii*) the DAF-9–DAs–DAF-12 pathway regulates LD growth/lipogensis rather than LD fusion. These functional differences also correlate with the facts that CYP-37A1 is expressed and functions in intestine while the DA-synthesis enzymes DAF-9 and DAF-36 are mainly in hypodermis (9, 10).

To our knowledge, the CYP-37A1–hormone–DAF-12 pathway described here constitutes a second *C. elegans* nuclear receptor pathway for which both the hormone synthesis enzyme and cognate nuclear receptor are identified, and for which evidence of an endogenous hormone ligand is provided. Our results also suggest that this hormonal pathway may interact with the DA pathway at the DAF-12 level. It is possible but unlikely that CYP-37A1-EMB-8 and DAF-12 act in parallel and the metabolite synthesized by CYP-37A1-EMB-8 is not a hormone ligand for DAF-12. This alternative scenario still predicts a novel non-DA hormone DAF-12.

Among nuclear receptors, DAF-12 is evolutionarily basal (31). DAF-12 may have adapted to sense multiple hormone ligands and carry out pleiotropic physiological functions before the proliferation of nuclear receptors during evolution. This kind of adaptation may allow the poikilothermic *C. elegans* to survive diverse environmental stresses (e.g., temperature stress). Thus, it is interesting that dysfunction of the CYP-37A1–hormone–DAF-12 pathway results in not only thermosensitive LD fusion but also a better tolerance of a high temperature of 34 °C, a longer lifespan at a moderately high temperature of 25 °C, and a reduced reproduction rate (19). It suggests that *C. elegans* in the wild may use this pathway to balance individual survival and reproduction (population survival) according to environment temperature. Similar environment temperature-regulated adaptation responses include the DAF-9–DAs–DAF-12 pathway-regulated dauer formation and the PARQ-2 (adiponectin receptor)-regulated fatty acid unsaturation (6–13, 32, 33).

Perhaps what is more interesting is that the thermosensitive LD fusion process regulated by the CYP-37A1–hormone–DAF-12 pathway is analogous to the temperature-dependent interconversion of beige/brown adipocytes (with multilocular LDs and active lipolysis) and white adipocytes (with unilocular LD and reduced lipolysis) in mammals (34). In other eukaryotic systems, multilocular LDs convert to unilocular LD through direct fusion (typical fusion), which has been regarded as a purely biophysical coalescence process affected by LD surface phospholipid composition (35–37). Another mode of multilocular-to-unilocular conversion is the asymmetrical transfer of TAG from one LD to another (atypical fusion) through the pore formed by the Cidec protein complex (38, 39). Neither of these processes is known to be temperature-dependent.

In contrast, the LD fusion process uncovered by the *cyp-37A1/emb-8* mutants differs in several respects to typical fusion and atypical fusion. First, it is dependent on environment temperature. Second, it has an optimal reaction temperature with a first-order kinetics typical of an enzymatic reaction, which is not predicted by a pure biophysical coalescence model (typical fusion). Third, it is not accompanied by an increase in TAG levels, although we cannot exclude the possibility of complementary changes in TAG synthesis and TAG hydrolysis in *cyp-37A1/emb-8*, that maintain TAG levels constant. In contrast, both typical fusion and atypical fusion were found to be accompanied by an increase of TAG levels (37, 40, 41). Fourth, it is not accompanied by detectable changes in phospholipids. Fifth, the *C. elegans* genome does not encode an apparent Cidea/Cidec homolog. These differences indicate that the thermosensitive LD fusion in *C. elegans* may involve a novel mechanism. However, it remains possible that the thermosensitive LD fusion shares some common mechanistic aspects with typical LD fusion, as both modes of fusion are fast and not asymmetric. For example, it could be that at 20 °C, *cyp-37A1/emb-8* has already changed the LD membrane phospholipid or fatty acid composition so as to alter membrane fluidity, but that the higher temperature is required to facilitate fusion. We have not been able to obtain evidence to support this hypothesis, which was shown to be the basis of typical LD fusion (35, 37).

Given the conservation of the CYP-37A1–hormone–DAF-12 pathway components between nematode and human, it is tempting to make predictions for human physiology and pathophysiology. First, the in vivo function of CYP4V2, the human ortholog of CYP-37A1, may be for the synthesis of a hormone that acts on a nuclear receptor (VDR, LXR, or FXR), dysfunction of which results in LD fusion and supersized LD/"lipid inclusion" formation in RPEs. Second, potential BCD risk factors include eye temperature, nuclear receptor mutations not yet identified, and POR polymorphisms already identified in "normal" human subjects (42). Finally, because CYP4V2 is broadly expressed in many human organs (26), the DAF-12-equivalent nuclear receptor may also be expressed and function in these organs to negatively regulate LD fusion. Dysfunction of this regulatory pathway may be associated with as yet unidentified diseases.

Materials and Methods

***C. elegans* Strains and Culture Conditions.** The WT *C. elegans* was N2 Bristol. All strains were grown on OP50 *E. coli*-seeded NGM plates. The growth temperature was 20 °C if not otherwise indicated. Mid- to late-L4–stage animals were used for phenotype characterization. For temperature-shift experiments, animals were grown continuously at 15 °C or 20 °C and were then shifted to 30 °C for 4 h to reach the mid-L4 stage. Mid-L4–stage animals were picked out and assayed for LD phenotype. Strains used in this study can be found in *SI Materials and Methods*.

Molecular Cloning of *drop-1* and *drop-8*. *drop-1(ssd2)* and *drop-8(ssd89)* were previously mapped onto an LG II 21.39 ~22.38 map unit and LG III −2.21 ~ −0.75 map unit, respectively (19). Genomic DNAs of the two strains were subjected to whole-genome resequencing and single nucleotide variance (SNV) and insertion/deletion (Indel) analysis. *drop-1* and *drop-8* were found to be *cyp-37A1* and *emb-8* mutations, respectively (*SI Materials and Methods*).

Noncomplementation Screen of *emb-8* Alleles. N2 males were mutagenized with ethylmethanesulfonate (EMS) and were used to mate *unc-32(e189) emb-8(ssd89)* hermaphrodites. Non-Unc F1 progeny with supersized LD phenotype were isolated. The *emb-8* locus of candidate isolates was PCR amplified and Sanger-sequenced for mutation (*SI Materials and Methods*).

***cyp-37A1* Suppressor Screen and Molecular Cloning of *drop-31*.** *cyp-37A1(ssd9)* and *cyp-37A1(ok673)* were mutagenized with EMS. F2 progeny were screened for the absence of the supersized LD phenotype. A total of 35 mutants were obtained and were tested for complementation. Two isolates, *ssd155* and *ssd240*, were found to belong to the same group *drop-31*. *drop-31(ssd155)* was subjected to SNP-based mapping and whole-genome resequencing, and was found to be a *daf-12* mutation. See *SI Materials and Methods* for more details.

Additional methods can be found in *SI Materials and Methods*.

ACKNOWLEDGMENTS. We thank Dr. David Weisblat for constructive comments on this manuscript; Drs. Gian Garriga, Yikun He, Legong Li, Peng Li, and Xiao Liu for useful discussions; Shuang Zhou for technical assistance; all members of our laboratory for discussion; Dr. Nengsheng Ye for helping us to use his gas chromatography instrument; Drs. X. Liu and G. Garriga for facilitating some of the imaging experiments; and Drs. E. Jorgensen and B. Liang for reagents and strains. Some other strains were provided by the *Caenorhabditis* Genetics Center, which is funded by National Institute of Health Office of Research Infrastructure Programs (P40 OD010440). This work was supported by National Natural Science Foundation of China Grant 31370820 (to S.O.Z.) and Beijing Municipal Education Commission Grant KZ201410028032 (to S.O.Z.). S.L. was supported in part by an International Exchange and Joint Training Grant of the Graduate School of Capital Normal University.

1. Nebert DW, Wikvall K, Miller WL (2013) Human cytochromes P450 in health and disease. *Philos Trans R Soc Lond B Biol Sci* 368:20120431.
2. Evans RM, Mangelsdorf DJ (2014) Nuclear receptors, RXR, and the Big Bang. *Cell* 157: 255–266.
3. Gissendanner CR, Crossgrove K, Kraus KA, Maina CV, Sluder AE (2004) Expression and function of conserved nuclear receptor genes in *Caenorhabditis elegans*. *Dev Biol* 266: 399–416.
4. Menzel R, Bogaert T, Achazi R (2001) A systematic gene expression screen of *Caenorhabditis elegans* cytochrome P450 genes reveals CYP35 as strongly xenobiotic inducible. *Arch Biochem Biophys* 395:158–168.
5. Rappleye CA, Tagawa A, Le Bot N, Ahringer J, Aroian RV (2003) Involvement of fatty acid pathways and cortical interaction of the pronuclear complex in *Caenorhabditis elegans* embryonic polarity. *BMC Dev Biol* 3:8.
6. Antebi A, Yeh WH, Tait D, Hedgecock EM, Riddle DL (2000) daf-12 encodes a nuclear receptor that regulates the dauer diapause and developmental age in *C. elegans*. *Genes Dev* 14:1512–1527.
7. Motola DL, et al. (2006) Identification of ligands for DAF-12 that govern dauer formation and reproduction in *C. elegans*. *Cell* 124:1209–1223.
8. Mahanti P, et al. (2014) Comparative metabolomics reveals endogenous ligands of DAF-12, a nuclear hormone receptor, regulating *C. elegans* development and lifespan. *Cell Metab* 19:73–83.
9. Gerisch B, Weitzel C, Kober-Eisermann C, Rottiers V, Antebi A (2001) A hormonal signaling pathway influencing *C. elegans* metabolism, reproductive development, and life span. *Dev Cell* 1:841–851.
10. Rottiers V, et al. (2006) Hormonal control of *C. elegans* dauer formation and life span by a Rieske-like oxygenase. *Dev Cell* 10:473–482.
11. Wollam J, et al. (2012) A novel 3-hydroxysteroid dehydrogenase that regulates reproductive development and longevity. *PLoS Biol* 10:e1001305.
12. Ludewig AH, et al. (2004) A novel nuclear receptor/coregulator complex controls *C. elegans* lipid metabolism, larval development, and aging. *Genes Dev* 18:2120–2133.
13. Gerisch B, et al. (2007) A bile acid-like steroid modulates *Caenorhabditis elegans* lifespan through nuclear receptor signaling. *Proc Natl Acad Sci USA* 104:5014–5019.
14. Russell DW (2003) The enzymes, regulation, and genetics of bile acid synthesis. *Annu Rev Biochem* 72:137–174.
15. Wang Z, et al. (2015) The nuclear receptor DAF-12 regulates nutrient metabolism and reproductive growth in nematodes. *PLoS Genet* 11:e1005027.
16. Martin S, Parton RG (2006) Lipid droplets: A unified view of a dynamic organelle. *Nat Rev Mol Cell Biol* 7:373–378.
17. Zhang SO, et al. (2010) Genetic and dietary regulation of lipid droplet expansion in *Caenorhabditis elegans*. *Proc Natl Acad Sci USA* 107:4640–4645.
18. Zhang SO, Trimble R, Guo F, Mak HY (2010) Lipid droplets as ubiquitous fat storage organelles in *C. elegans*. *BMC Cell Biol* 11:96.
19. Li S, et al. (2016) A genetic screen for mutants with supersized lipid droplets in *Caenorhabditis elegans*. *G3 (Bethesda)* 6:2407–2419.
20. Frøkjaer-Jensen C, et al. (2008) Single-copy insertion of transgenes in *Caenorhabditis elegans*. *Nat Genet* 40:1375–1383.
21. Xu N, et al. (2012) The FATP1-DGAT2 complex facilitates lipid droplet expansion at the ER-lipid droplet interface. *J Cell Biol* 198:895–911.
22. Walker AK, et al. (2011) A conserved SREBP-1/phosphatidylcholine feedback circuit regulates lipogenesis in metazoans. *Cell* 147:840–852.
23. Klemm RW, et al. (2013) A conserved role for atlastin GTPases in regulating lipid droplet size. *Cell Reports* 3:1465–1475.
24. Stenico M, Lloyd AT, Sharp PM (1994) Codon usage in *Caenorhabditis elegans*: Delineation of translational selection and mutational biases. *Nucleic Acids Res* 22: 2437–2446.
25. Bietti G (1937) Ueber familiaeres vorkommen von "retinitispunctata albescens" (verbunden mit "dystrophia marginalis cristallinea corneae"), glitzern des glaskoerpers und anderen degenerativen augenveraenderungen. *Klin Mbl Augenheilk* 99:737–757.
26. Li A, et al. (2004) Bietti crystalline corneoretinal dystrophy is caused by mutations in the novel gene CYP4V2. *Am J Hum Genet* 74:817–826.
27. Nakano M, Kelly EJ, Rettie AE (2009) Expression and characterization of CYP4V2 as a fatty acid omega-hydroxylase. *Drug Metab Dispos* 37:2119–2122.
28. Nakano M, Kelly EJ, Wiek C, Hanenberg H, Rettie AE (2012) CYP4V2 in Bietti's crystalline dystrophy: Ocular localization, metabolism of ω-3-polyunsaturated fatty acids, and functional deficit of the p.H331P variant. *Mol Pharmacol* 82:679–686.
29. Kelly EJ, Nakano M, Rohatgi P, Yarov-Yarovoy V, Rettie AE (2011) Finding homes for orphan cytochrome P450s: CYP4V2 and CYP4F22 in disease states. *Mol Interv* 11: 124–132.
30. Lockhart CM, Nakano M, Rettie AE, Kelly EJ (2014) Generation and characterization of a murine model of Bietti crystalline dystrophy. *Invest Ophthalmol Vis Sci* 55: 5572–5581.
31. Robinson-Rechavi M, Maina CV, Gissendanner CR, Laudet V, Sluder A (2005) Explosive lineage-specific expansion of the orphan nuclear receptor HNF4 in nematodes. *J Mol Evol* 60:577–586.
32. Svensk E, et al. (2013) PAQR-2 regulates fatty acid desaturation during cold adaptation in *C. elegans*. *PLoS Genet* 9:e1003801.
33. Ma DK, et al. (2015) Acyl-CoA dehydrogenase drives heat adaptation by sequestering fatty acids. *Cell* 161:1152–1163.
34. Bartelt A, Heeren J (2014) Adipose tissue browning and metabolic health. *Nat Rev Endocrinol* 10:24–36.
35. Krahmer N, et al. (2011) Phosphatidylcholine synthesis for lipid droplet expansion is mediated by localized activation of CTP:phosphocholine cytidylyltransferase. *Cell Metab* 14:504–515.
36. Szymanski KM, et al. (2007) The lipodystrophy protein seipin is found at endoplasmic reticulum lipid droplet junctions and is important for droplet morphology. *Proc Natl Acad Sci USA* 104:20890–20895.
37. Fei W, et al. (2011) A role for phosphatidic acid in the formation of "supersized" lipid droplets. *PLoS Genet* 7:e1002201.
38. Gong J, et al. (2011) Fsp27 promotes lipid droplet growth by lipid exchange and transfer at lipid droplet contact sites. *J Cell Biol* 195:953–963.
39. Puri V, et al. (2008) Cidea is associated with lipid droplets and insulin sensitivity in humans. *Proc Natl Acad Sci USA* 105:7833–7838.
40. Puri V, et al. (2007) Fat-specific protein 27, a novel lipid droplet protein that enhances triglyceride storage. *J Biol Chem* 282:34213–34218.
41. Guo Y, et al. (2008) Functional genomic screen reveals genes involved in lipid-droplet formation and utilization. *Nature* 453:657–661.
42. Pandey AV, Sproll P (2014) Pharmacogenomics of human P450 oxidoreductase. *Front Pharmacol* 5:103.